Anisotropic Two-Dimensional Screening at the Surface of Black Phosphorus

Brian Kiraly,[1] Elze J. Knol,[1] Klara Volckaert,[2] Deepnarayan Biswas,[2] Alexander N. Rudenko,[3,1,4] Danil A. Prishchenko,[4] Vladimir G. Mazurenko,[4] Mikhail I. Katsnelson,[1,4] Philip Hofmann,[2] Daniel Wegner,[1] and Alexander A. Khajetoorians[1]
[1]*Institute for Molecules and Materials, Radboud University, Nijmegen 6525AJ, Netherlands*
[2]*Department of Physics and Astronomy, Interdisciplinary Nanoscience Center, Aarhus University, 8000 Aarhus C, Denmark*
[3]*School of Physics and Technology, Wuhan University, Wuhan 430072, China*
[4]*Theoretical Physics and Applied Mathematics Department, Ural Federal University, 620002 Ekaterinburg, Russia*

(Received 1 July 2019; published 21 November 2019)

Electronic screening can have direct consequences for structural arrangements on the nanoscale, such as on the periodic ordering of adatoms on a surface. So far, such ordering phenomena have been explained in terms of isotropic screening of free electronlike systems. Here, we directly illustrate the structural consequences of anisotropic screening, making use of a highly anisotropic two-dimensional electron gas (2DEG) near the surface of black phosphorous. The presence of the 2DEG and its filling is controlled by adsorbed potassium atoms, which simultaneously serve to probe the electronic ordering. Using scanning tunneling microscopy, we show that the anisotropic screening leads to the formation of potassium chains with a well-defined orientation and spacing. We quantify the mean interaction potential utilizing statistical methods and find that the dimensionality and anisotropy of the screening is consistent with the presence of a band bending-induced 2DEG near the surface. The electronic dispersion of the 2DEG inferred by electronic ordering is consistent with that measured by angle-resolved photoemission spectroscopy.

DOI: 10.1103/PhysRevLett.123.216403

The role of screening in materials with reduced dimensionality has recently seen renewed interest due to the possibilities arising from single-layer van der Waals materials, which can be stacked into complex heterostructures [1–3] and/or tuned through their dielectric environment [4,5]. Experimentally, the effect of screening is particularly accessible at the surface of a material, where it has been shown that two-dimensional Friedel oscillations have direct consequences on structural adatom ordering [6–18], as well as on the modulation of adatom diffusion barriers [19]. Scanning tunneling microscopy (STM) has also been utilized to quantify the screened Coulomb potential at the surface of semiconductors [18] and to disentangle the contributions of free electrons from band-bending induced quantum well states to the screened potential in topological insulators [16]. In all of these cases, the resulting effects can be explained in terms of an isotropic electronic dispersion responsible for the screening, i.e., a free electronlike system with an isotropic length of k_F. While Friedel oscillations for anisotropic [20] or spin-split [21] Fermi contours have been observed, the consequences of anisotropic screening on ordering are still not well understood.

Black phosphorus (BP) is a layered semiconductor that offers the unique opportunity to explore adsorbate ordering in the presence of anisotropic screening [22–26]. The structure of BP is highly anisotropic, leading to strong consequences in the band structure [27,28] as well as its expected dielectric response [26], providing a promising platform to quantify the effects of anisotropic screening. Here, we quantify the electrostatic screening from the surface layers of BP by looking at the effects on the long-range ordering of charged potassium adatoms. Utilizing STM, we explore the spatial distributions of potassium adatoms as a function of temperature (T) and potassium density (n_K). STM imaging reveals the development of 1D potassium structures, strongly favoring an orientation along the armchair direction, driven by anisotropic charge screening. Using STM images, we quantify the mean interaction potential (E_m) [8,9,16] and corroborate changes to E_m with measurements of the two-dimensional (2D) Fermi contour derived from angle-resolved photoemission spectroscopy (ARPES). We observe very long-ranged, anisotropic screening behavior. While Friedel oscillation-related screening behavior accounts for the long-range ordering in both directions, additional short-range correlations are observed along the armchair direction.

An STM image of a clean BP surface after cleaving *in situ* is shown in Fig. 1(a). Characteristic intrinsic defects are observed at and below the surface [29], with an areal density of approximately $n_V = 3.1 \times 10^{10}$ cm^{-2}. The inset shows the pristine crystal lattice, with the x (armchair/[100]) and y (zigzag/[010]) directions labeled. The surface after low-temperature deposition of K atoms ($n_K = 7.0 \times 10^{11}$ cm^{-2}) is shown in Fig. 1(b). The adatoms are imaged as isotropic protrusions with a bias-dependent apparent height 200 pm $< \Delta z <$ 300 pm. As shown in Fig. 2, the diffusion of K adatoms at the surface of BP occurs between $T = 4.4$

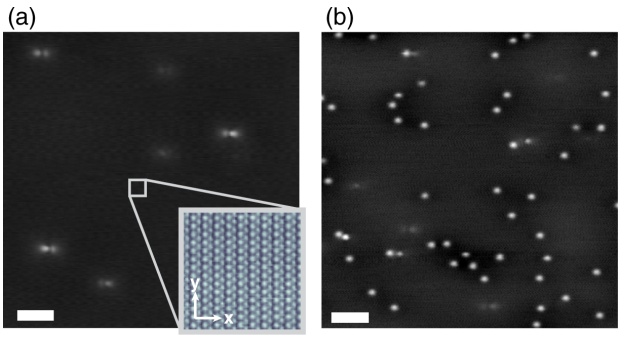

FIG. 1. Clean and K-doped black phosphorus. (a) STM constant-current image showing pristine black phosphorus with characteristic vacancies ($V_s = -400$ mV, $I_t = 20$ pA, scale bar = 10 nm). The inset shows an atomically resolved image of the black phosphorus surface ($V_s = -100$ mV, $I_t = 40$ pA). The notation used here is armchair $= x = [100]$ and zigzag $= y = [010]$. (b) K-doped black phosphorus at areal adatom density $n_K = 7.0 \times 10^{11}$ cm^{-2} after low-temperature deposition at $T = 4.4$ K. K adatoms appear as isotropic protrusions with an apparent height of approximately 200 pm ($V_s = 1$ V, $I_t = 10$ pA, scale bar = 10 nm).

and 5.6 K, indicating an extremely low lateral diffusion barrier (see also the Supplemental Material, Fig. S1 [30]) [31–38]. In order to ensure negligible tip-induced atomic motion, most of the topographic measurements in this work were performed with small currents ($I_t < 6$ pA). At these currents, we were not able to atomically resolve the BP lattice while leaving the K adatoms unperturbed.

Adsorption of alkali adatoms usually leads to charge transfer to the substrate. In the case of adsorption on a semiconductor surface, this can result in substantial band bending. This was confirmed here by observing a shift of the band edges with respect to E_F (see Fig. S2 and S3 [30]) [29,39–41]. A sufficiently strong band bending can lead to confinement of the conduction band (CB) states near the surface, as already reported for both BP [27,42], as well as other narrow band gap semiconductors [43,44]. In the case of BP, the resulting 2DEG reflects the strong electronic anisotropy of the CB [27], and we can thus expect this electronic structure to be a model system for studying the effect of screening in a strongly anisotropic 2D system.

To study the resultant screened interaction between the positively charged K adatoms, we characterized the relative positions of large numbers (ca. 10 000) of adatoms $[g(x, y)]$ in order to calculate the vector-resolved pair distribution function $[g(x, y)/g_{\mathrm{ran}}(x, y)]$, where $g_{\mathrm{ran}}(x, y)$ is the distribution expected for random adsorption sites (see Fig. S4 [30]). The mean interaction potential is then straightforwardly calculated from the pair distribution function via the reversible work theorem as $E_m(x, y) = -k_B T \ln[g(x, y)/g_{\mathrm{ran}}(x, y)]$. The mean interaction potential quantifies the spatially dependent potential energy landscape felt by a given adatom with respect to a homogeneous background distribution. Extraction of the mean interaction potential has been utilized to study dopant distributions in semiconductors [45], the role of dimensionality in screened Coulomb interactions in a variety of materials [11,16], and free carrier-mediated interactions at metallic surfaces [8,9]. We note that this is different from the pair interaction potential, which quantifies the potential energy between two adatoms. Extraction of the pair interaction potential from the mean interaction potential requires an additional approximation, which is only typically appropriate in the case that the interaction is short ranged [16]. In order to probe the effect of screening, we first examined the adsorbate distribution upon adsorption at $T = 4.4$ K; we then monitored changes to the distribution after annealing the sample to higher temperatures (T_{anneal}) in order to overcome surface diffusion barriers (Fig. S1 [30]). During the annealing process, the screened interaction potential plays a strong role in the redistribution of K atoms, which can then be observed after cooling again to the measurement temperature of 4.4 K. We also note that the temperature used to derive E_m is a lower bound as we do not probe higher temperatures, although we observe qualitatively similar distributions at higher, uncalibrated, annealing temperatures.

The distribution of K adatoms ($n_K = 2.0 \times 10^{12}$ cm^{-2}) after low-temperature deposition ($T = 4.4$ K) is shown in Fig. 2(a). While the large-scale STM image clearly shows a lack of long-range order, the corresponding plot of E_m in Fig. 2(e) demonstrates short-range repulsion (red) at atomic separations less than 2 nm. This is ascribed to a short-range Coulomb interaction mediated by the substrate. As the sample is annealed, clear anisotropic ordering emerges [Figs. 2(b)–2(d)]. Examining the STM image from Fig. 2(b) ($T_{\mathrm{anneal}} = 5.6$ K), chainlike structures composed of a few adatoms develop, oriented along the x direction. After annealing to higher temperatures [$T_{\mathrm{anneal}} = 8.0$ K for Fig. 2(c) and $T_{\mathrm{anneal}} = 14.8$ K for Fig. 2(d)] the chains extend in length (along the x direction) and show a characteristic interchain separation along the y direction. It is noteworthy that the chains orient orthogonal to the direction along which the diffusion barrier is lower, demonstrating that this ordering is not driven by diffusion energy barriers (Fig. S1 [30]). The development of long-range order seen prominently in Figs. 2(c) and 2(d) is clearly reflected in the plots of E_m [Figs. 2(g) and 2(h)], where deep attractive regions (blue) appear in the x direction (indicating a high likelihood of finding neighboring atoms at such a position) and oscillatory interactions emerge along y.

To further analyze the potential landscape, line profiles along the y direction ($x = 0$) taken from the plots of E_m in Figs. 2(e)–2(h) are shown in Fig. 2(j). The annealing temperature-dependent line profiles along y reveal clear oscillations up to distances of nearly 40 nm from the origin. While the oscillation amplitude increases with annealing temperature (notably from $T_{\mathrm{anneal}} = 8.0$ to

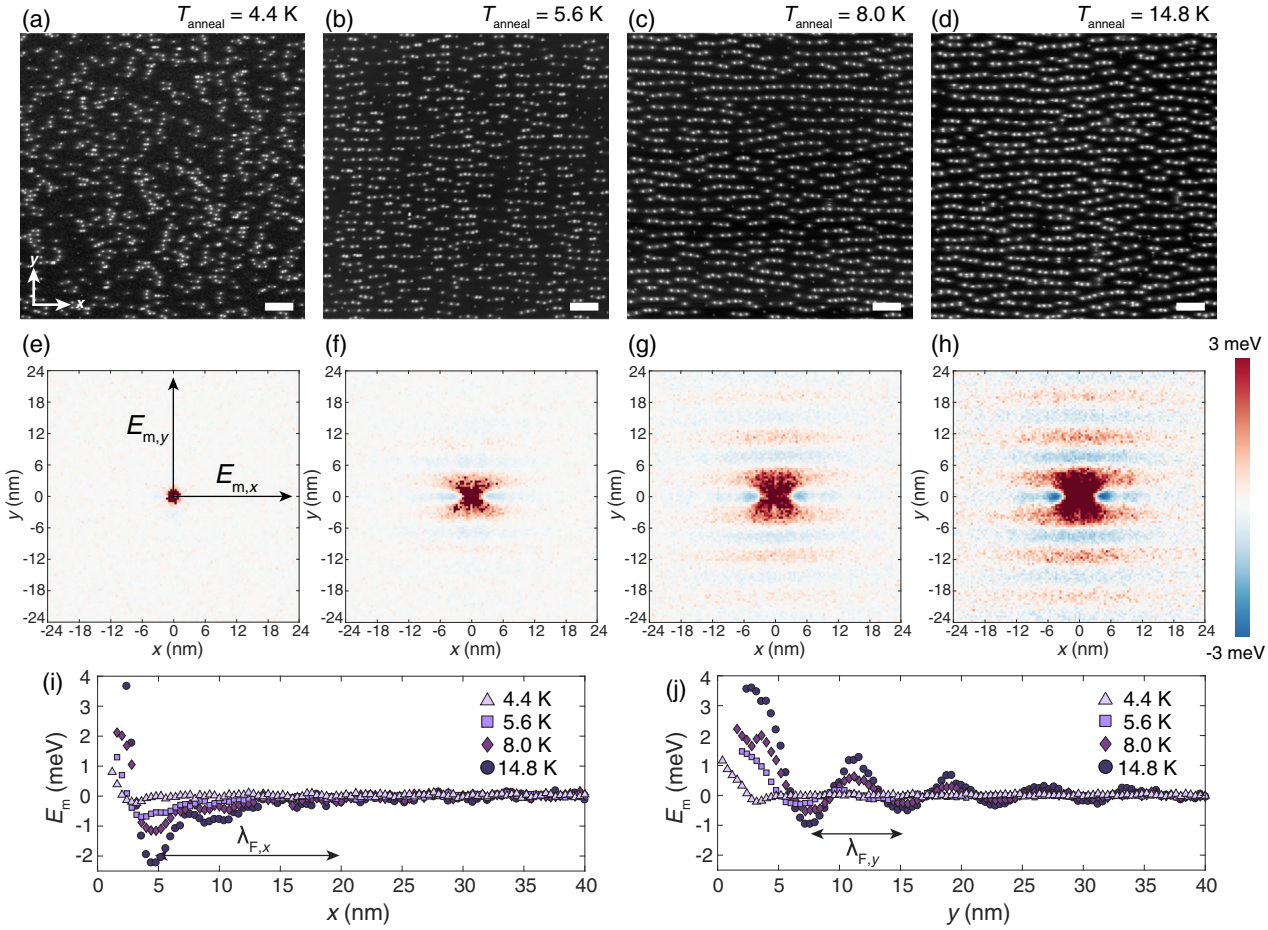

FIG. 2. Temperature-dependent distribution of K adatoms. (a) Large-scale STM constant-current image of K-doped BP (adatom density $n_K = 2.0 \times 10^{12}$ cm^{-2}) after low-temperature deposition at $T = 4.4$ K ($V_s = -1$ V, $I_t = 3$ pA, scale bar = 20 nm). The x,y orientation refers to the atomic lattice in Fig. 1(a) and is the same for (b)–(d). (b)–(d) STM constant current images taken at $T = 4.4$ K after annealing the K-doped BP sample for ten minutes to $T_{anneal} = 5.6$ K, 8.0 K, and 14.8 K, respectively ($V_s = -1$ V, $I_t = 3$ pA, scale bar = 20 nm). (e)–(h) Mean interaction potentials for single K dopant at (0,0) calculated from multiple images. Line cuts from mean interaction potential (i) along x and (j) along y. The arrows in (e) refer to the directions of these line cuts.

$T_{anneal} = 14.8$ K), the oscillatory period remains unchanged. The fact that the ordering is periodic points to an interaction potential that is strongly influenced by Friedel oscillations along y, as seen for isotropic interactions in other systems [8,9]. As we show later, the observed periodicity is indeed consistent with Fermi wavelength along the y direction ($\lambda_{F,y}$). Also, doping-induced changes of the ordering can be explained by corresponding modifications of the Fermi surface as a function of electron filling.

The behavior of E_m along x [Fig. 2(i)], is strikingly different from y [Fig. 2(j)]. The interatomic spacing between atoms in the 1D chains can be ascribed to a prominent potential minimum approximately 4 nm from the origin, as well as a second weaker minimum at 8 nm. However, these structures cannot be reconciled with Friedel oscillations, because they appear at distances much shorter than $\lambda_{F,x}$ [see Fig. 2(i)]. Explaining the atomic separation along the chain thus requires a more sophisticated treatment of the K-doped BP dielectric function to describe the screened Coulomb interactions, along with a consideration of the preferred adsorption positions on the lattice. However, weak manifestations of Friedel-type interactions can still be observed in the x direction, because half the Fermi wavelength ($\lambda_{F,x}/2 = 15 \pm 6$ nm) determined from ARPES coincides with the characteristic finite length of the chains (see Fig. S5 [30]).

The interpretation of the observed ordering in terms of Friedel oscillations can be further confirmed by coverage-dependent measurements in which the filling and Fermi vectors of the 2DEG are changed. Figure 3 shows a series of interaction potentials obtained from different potassium coverages, collected after annealing at temperatures between 14 and 18 K. At $n_K = 7.0 \times 10^{11}$ cm^{-2}, the mean interaction potential [Fig. 3(a) for STM images, see Fig. S6 [30]] clearly lacks the pronounced anisotropy

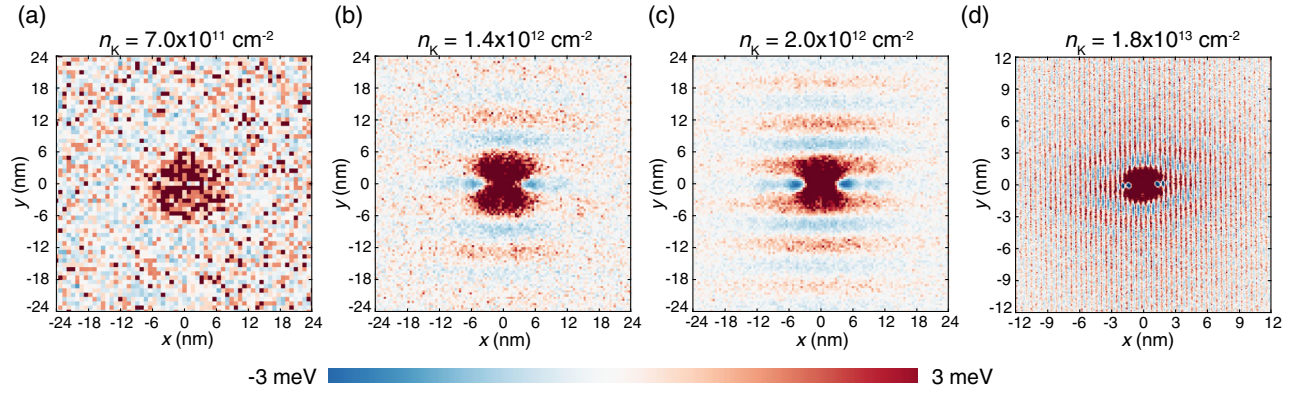

FIG. 3. Density-dependent mean interaction potentials. Mean interaction potentials for varying K adatom density (n_K) are shown after annealing the samples to 13.4 K (lowest density), 14.8 K (medium and high density), and approximately 18.0 K (highest density). (a) Mean interaction potential for lowest K density ($n_K = 7.0 \times 10^{11}$ cm^{-2}) showing isotropic screening behavior. (b) Mean interaction potential at $n_K = 1.4 \times 10^{12}$ cm^{-2}, revealing the onset of screening anisotropy. (c),(d) Mean interaction potential for $n_K = 2.0 \times 10^{12}$ cm^{-2} and $n_K = 1.8 \times 10^{13}$ cm^{-2}, respectively.

seen for higher coverages in Figs. 3(b)–3(d) and Fig. 2(h). The potential is repulsive at short range and shows a weakly attractive region at around 11 nm. We note that at this coverage we cannot deduce the potential with high precision. With increasing coverage ($n_K \geq 1.4 \times 10^{12}$ cm^{-2}), there is a qualitative change which can be explained by the CB minimum crossing E_F. Beyond this coverage, E_m remains qualitatively similar, but as we show in more detail below, small changes in the characteristic periodicity appear that can be linked to the doping-dependent filling of the 2DEG [inset Fig. 4(a)].

For a detailed analysis of the doping-dependent changes, as well as the dimensionality of the screening, we analyze the decay of the oscillation in the y direction [Fig. 4(a)]. A radially symmetric interaction potential derived from an electron gas with an isotropic Fermi surface can be described by [46]

$$E_m(R) = -C\frac{\cos(2k_F R + \delta)}{(k_F R)^m}, \qquad (1)$$

where C is a constant, k_F is the characteristic Fermi surface wave vector, R is the distance to the scattering center, δ is the phase shift upon scattering, and m is the spatial dimensionality. We fit the oscillatory E_m data in Fig. 4(a) to Eq. (1), obtaining the scattering wave vectors $q_y = 2 * k_{F,y}$, phase shifts, and dimensionality m (see Fig. S7 in the Supplemental Material [30] for further details). For the highest doping level ($n_K = 1.8 \times 10^{13}$ cm^{-2}, see Figs. S8 and S9 [30]) [25,47], the best fit is obtained using $m = 2$, resulting in $q_y = 0.28 \pm 0.02$ Å^{-1}. The profiles taken from lower doping levels [$n_K = 2.0 \times 10^{12}$ cm^{-2} (red points) and $n_K = 1.4 \times 10^{12}$ cm^{-2} (blue points)] result in $q_y = 0.08 \pm 0.01$ and $q_y = 0.07 \pm 0.01$ Å^{-1}, respectively. As seen in Fig. 4(a), these data show a much slower decay in the oscillatory E_m. In fact, taking $m = 1$ provides a better fit to this data (red and blue lines, respectively), indicating a quasi-one-dimensional screening along k_y. This observed scattering dimensionality could be related to anisotropic charge puddling around the K dopants or Fermi surface nesting, but the origin is not clear from this formalism.

In order to independently confirm both the Fermi contour dimensions and dimensionality of the states near E_F, we perform doping-dependent ARPES measurements (see Fig. S10 [30]) [48]. The band structure of K-doped BP ($n_{2D} = 1.49 \times 10^{13}$ cm^{-2}) is shown in Figs. 4(b) and 4(c). To confirm the 2D confinement of the bands near E_F, data are collected as a function of photon energy, demonstrating a clear lack of k_z dispersion (Fig. S11 [30]). The ARPES measurements reaffirm the indications from STM measurements that K-doped BP hosts a 2D electron system at the surface, corroborating the previous conclusions from ARPES experiments [27,42,49]. Furthermore, the 2D bands show anisotropy and effective masses (Fig. S12 [30]) roughly consistent with expectations for both monolayer and bulk BP [50]. Using Luttinger's theorem [51] to extract the carrier density (n_{2D}) from ARPES band structure, we compare the observed Fermi surface vectors ($k_{F,x}$ and $k_{F,y}$) with those obtained from STM (under the assumption $n_K = n_{2D}$), as shown in Fig. 4(d). Note that the K coverage for the determination of the conduction band-related Fermi contour from ARPES is significantly larger than the typical coverage in the STM experiments. The reason is that the conduction band-derived states need to be sufficiently populated in order to determine the detailed dispersion, since ARPES only probes occupied states. Nevertheless, the agreement for the extracted carrier densities between STM and ARPES is excellent. At low n_K (see Fig. S10 [30]), we do observe a band gap at E_F and rigid band shifts proportional to n_K, consistent with STS measurements (Fig. S2 [30]) and previous ARPES measurements [27].

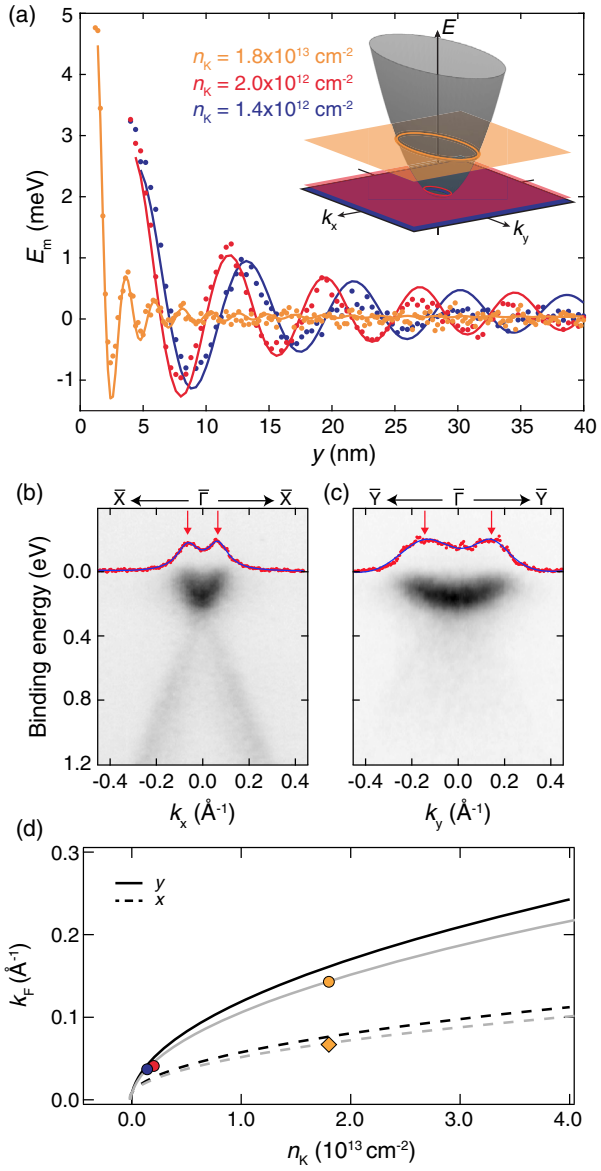

FIG. 4. Relation between electron filling and screening. (a) Line profiles of the oscillatory mean interaction potential along y for samples doped with $n_K = 1.4 \times 10^{12}$ cm^{-2} (dark blue), $n_K = 2.0 \times 10^{12}$ cm^{-2} (red), and $n_K = 1.8 \times 10^{13}$ cm^{-2} (orange). Points indicate measured data from Fig. 3, while the solid lines show fits of the data to Eq. (1) described in the text. (Inset) Illustration of the anisotropic CB of BP with colored slices indicating doping levels from Figs. 3 and 4(a). (b) and (c) ARPES data taken after dosing K onto BP with $n_K = 1.5 \times 10^{13}$ cm^{-2} showing a 2D electronlike band along (b) $\bar{\Gamma} - \bar{X}$ and (c) $\bar{\Gamma} - \bar{Y}$ directions. Momentum distribution cuts (red) at E_F show distinct k_F peaks (red arrows) that yield $2 * k_{F,y} = 0.28$ Å^{-1} and $2 * k_{F,x} = 0.13$ Å^{-1}, respectively. (d) Comparison of the Fermi wave vectors along $\bar{\Gamma} - \bar{X}$ and $\bar{\Gamma} - \bar{Y}$ as a function of potassium density (n_K) for ARPES data (solid and dashed lines) and STM data (points). The coverage for the ARPES data in (b) and (c) approximately corresponds to the orange markers of the STM data. Dopant density for ARPES data was calculated using Luttinger's theorem under the assumption that a single electron per K atom is transferred to the BP surface layer (black) and 0.8 electrons are transferred (gray).

In conclusion, we demonstrate that K doping of the BP surface reveals the anisotropic in-plane screening and quasi-1D ordering of K adatoms mediated by the 2DEG induced by band bending. By examining large arrays of interacting K adatoms on the surface of BP, we show that the anisotropic screened Coulomb response governs the formation of 1D potassium chains and that the near-surface confined charge carriers mediate extremely long-ranged interchain interactions (>40 nm along the y direction), at relatively low carrier densities ($n_K = 2.0 \times 10^{12}$ cm^{-2}). The anisotropic response of the system persists to high carrier densities ($n_K = 1.8 \times 10^{13}$ cm^{-2}), allowing us to correlate the STM results with ARPES experiments. We note that the unusual interatomic spacing in a given K chain cannot be accounted for considering screening effects at long wavelength and requires a more sophisticated picture of the K-doped BP dielectric function. The results show that conduction electron-mediated interactions in BP are strongly anisotropic and extremely long ranged, which may have significant ramifications for excitonic excitations in BP.

The authors would like to acknowledge scientific discussions with Malte Rösner. E. K. and A. A. K. also acknowledge the VIDI project: "Manipulating the interplay between superconductivity and chiral magnetism at the single atom level" with Project No. 680-47-534, which is financed by NWO. B. K. and A. A. K. acknowledge support from the European Union's Horizon 2020 research and innovation programme under Grant Agreement No. 751437. A. A. K acknowledges support from the European Research Council (ERC) under the European Union's Horizon 2020 research and innovation programme (Grant Agreement No. 818399, SPINAPSE). M. I. K. acknowledges support from the Joint Transnational Call – Flagship European Research Area project GRANSPORT. This work was supported by VILLUM FONDEN via the Centre of Excellence for Dirac Materials (Grant No. 11744). A. N. R., D. A. P., and V. G. M. acknowledge support from the Russian Science Foundation, Grant No. 17-72-20041.

[1] A. K. Geim and I. V. Grigorieva, Nature (London) **499**, 419 (2013).
[2] Y. Cao, V. Fatemi, S. Fang, K. Watanabe, T. Taniguchi, E. Kaxiras, and P. Jarillo-Herrero, Nature (London) **556**, 43 (2018).
[3] K. L. Seyler, P. Rivera, H. Yu, N. P. Wilson, E. L. Ray, D. G. Mandrus, J. Yan, W. Yao, and X. Xu, Nature (London) **567**, 66 (2019).
[4] M. Rösner, C. Steinke, M. Lorke, C. Gies, F. Jahnke, and T. O. Wehling, Nano Lett. **16**, 2322 (2016).
[5] A. Raja *et al.*, Nat. Commun. **8**, 15251 (2017).
[6] J. Trost, T. Zambelli, J. Wintterlin, and G. Ertl, Phys. Rev. B **54**, 17850 (1996).
[7] T. T. Tsong, Phys. Rev. Lett. **31**, 1207 (1973).

[8] J. Repp, F. Moresco, G. Meyer, K.-H. Rieder, P. Hyldgaard, and M. Persson, Phys. Rev. Lett. **85**, 2981 (2000).
[9] N. Knorr, H. Brune, M. Epple, A. Hirstein, M. A. Schneider, and K. Kern, Phys. Rev. B **65**, 115420 (2002).
[10] T. Yokoyama, T. Takahasi, K. Shinozaki, and M. Okamoto, Phys. Rev. Lett. **98**, 206102 (2007).
[11] I. Fernandez-Torrente, S. Monturet, K. J. Franke, J. Fraxedas, N. Lorente, and J. I. Pascual, Phys. Rev. Lett. **99**, 176103 (2007).
[12] C. Liu, T. Uchihashi, and T. Nakayama, Phys. Rev. Lett. **101**, 146104 (2008).
[13] N. N. Negulyaev, V. S. Stepanyuk, L. Niebergall, P. Bruno, W. Auwärter, Y. Pennec, G. Jahnz, and J. V. Barth, Phys. Rev. B **79**, 195411 (2009).
[14] N. N. Negulyaev, V. S. Stepanyuk, L. Niebergall, P. Bruno, M. Pivetta, M. Ternes, F. Patthey, and W. D. Schneider, Phys. Rev. Lett. **102**, 246102 (2009).
[15] X. P. Zhang, B. F. Miao, L. Sun, C. L. Gao, A. Hu, H. F. Ding, and J. Kirschner, Phys. Rev. B **81**, 125438 (2010).
[16] P. Löptien, L. Zhou, J. Wiebe, A. A. Khajetoorians, J. L. Mi, B. B. Iversen, P. Hofmann, and R. Wiesendanger, Phys. Rev. B **89**, 085401 (2014).
[17] P. Ebert, T. Zhang, F. Kluge, M. Simon, Z. Zhang, and K. Urban, Phys. Rev. Lett. **83**, 757 (1999).
[18] P. Ebert, X. Chen, M. Heinrich, M. Simon, K. Urban, and M. G. Lagally, Phys. Rev. Lett. **76**, 2089 (1996).
[19] N. N. Negulyaev, V. S. Stepanyuk, L. Niebergall, P. Bruno, W. Hergert, J. Repp, K. H. Rieder, and G. Meyer, Phys. Rev. Lett. **101**, 226601 (2008).
[20] P. Hofmann, B. G. Briner, M. Doering, H. P. Rust, E. W. Plummer, and A. M. Bradshaw, Phys. Rev. Lett. **79**, 265 (1997).
[21] J. I. Pascual *et al.*, Phys. Rev. Lett. **93**, 196802 (2004).
[22] X. Ling, H. Wang, S. Huang, F. Xia, and M. S. Dresselhaus, Proc. Natl. Acad. Sci. U.S.A. **112**, 4523 (2015).
[23] L. Li, Y. Yu, G. J. Ye, Q. Ge, X. Ou, H. Wu, D. Feng, X. H. Chen, and Y. Zhang, Nat. Nanotechnol. **9**, 372 (2014).
[24] X. Wang, A. M. Jones, K. L. Seyler, V. Tran, Y. Jia, H. Zhao, H. Wang, L. Yang, X. Xu, and F. Xia, Nat. Nanotechnol. **10**, 517 (2015).
[25] T. Low, R. Roldán, H. Wang, F. Xia, P. Avouris, L. M. Moreno, and F. Guinea, Phys. Rev. Lett. **113**, 106802 (2014).
[26] D. A. Prishchenko, V. G. Mazurenko, M. I. Katsnelson, and A. N. Rudenko, 2D Mater. **4**, 025064 (2017).
[27] J. Kim, S. S. Baik, S. H. Ryu, Y. Sohn, S. Park, B.-G. Park, J. Denlinger, Y. Yi, H. J. Choi, and K. S. Kim, Science **349**, 723 (2015).
[28] A. N. Rudenko, S. Yuan, and M. I. Katsnelson, Phys. Rev. B **92**, 085419 (2015).
[29] B. Kiraly, N. Hauptmann, A. N. Rudenko, M. I. Katsnelson, and A. A. Khajetoorians, Nano Lett. **17**, 3607 (2017).
[30] See Supplemental Material at http://link.aps.org/supplemental/10.1103/PhysRevLett.123.216403 for methods, calculations of the potassium diffusion barrier, characterization of K-doping via scanning tunneling spectroscopy and first principles calculations, a detailed explanation for extracting the mean interaction potential, an analysis of interchain periodicities along x, STM constant-current images for the data shown in Fig. 3, additional information about the fits to the mean interaction potential in Fig. 4, STM constant-current images with $n_K = 1.8 \times 10^{13}$ cm^{-2} and theoretical predictions for Friedel oscillations, ARPES measurements of the band structure with varying n_K, the k_z band dispersion of the surface BP bands, and estimates for the anisotropic BP effective mass.
[31] S.-W. Kim, H. Jung, H.-J. Kim, J.-H. Choi, S.-H. Wei, and J.-H. Cho, Phys. Rev. B **96**, 075416 (2017).
[32] P. E. Blöchl, Phys. Rev. B **50**, 17953 (1994).
[33] G. Kresse and J. Furthmüller, Phys. Rev. B **54**, 11169 (1996).
[34] G. Kresse and D. Joubert, Phys. Rev. B **59**, 1758 (1999).
[35] J. P. Perdew, K. Burke, and M. Ernzerhof, Phys. Rev. Lett. **77**, 3865 (1996).
[36] J. Renard, M. B. Lundeberg, J. A. Folk, and Y. Pennec, Phys. Rev. Lett. **106**, 156101 (2011).
[37] K. T. Chan, J. B. Neaton, and M. L. Cohen, Phys. Rev. B **77**, 235430 (2008).
[38] K. Rytkönen, J. Akola, and M. Manninen, Phys. Rev. B **75**, 075401 (2007).
[39] B. Kiraly, A. N. Rudenko, W. M. J. van Weerdenburg, D. Wegner, M. I. Katsnelson, and A. A. Khajetoorians, Nat. Commun. **9**, 3904 (2018).
[40] N. Marzari, A. A. Mostofi, J. R. Yates, I. Souza, and D. Vanderbilt, Rev. Mod. Phys. **84**, 1419 (2012).
[41] A. A. Mostofi, J. R. Yates, Y-. S. Lee, I. Souza, D. Vanderbilt, and N. Marzari, Comput. Phys. Commun. **178**, 685 (2008).
[42] N. Ehlen, A. Sanna, B. V. Senkovskiy, L. Petaccia, A. V. Fedorov, G. Profeta, and A. Grüneis, Phys. Rev. B **97**, 045143 (2018).
[43] K. Hashimoto, C. Sohrmann, J. Wiebe, T. Inaoka, F. Meier, Y. Hirayama, R. A. Römer, R. Wiesendanger, and M. Morgenstern, Phys. Rev. Lett. **101**, 256802 (2008).
[44] M. Bianchi, D. Guan, S. Bao, J. Mi, B. B. Iversen, P. D. C. King, and P. Hofmann, Nat. Commun. **1**, 128 (2010).
[45] K.-J. Chao, C.-K. Shih, D. W. Gotthold, and B. G. Streetman, Phys. Rev. Lett. **79**, 4822 (1997).
[46] K. H. Lau and W. Kohn, Surf. Sci. **75**, 69 (1978).
[47] M. I. Katsnelson, *Graphene: Carbon in Two Dimensions* (Cambridge University Press, Cambridge, England, 2012).
[48] S. V. Hoffmann, C. Søndergaard, C. Schultz, Z. Li, and P. Hofmann, Nucl. Instrum. Methods Phys. Res., Sect. A **523**, 441 (2004).
[49] J. Kim, S. S. Baik, S. W. Jung, Y. Sohn, S. H. Ryu, H. J. Choi, B.-J. Yang, and K. S. Kim, Phys. Rev. Lett. **119**, 226801 (2017).
[50] S. Yuan, A. N. Rudenko, and M. I. Katsnelson, Phys. Rev. B **91**, 115436 (2015).
[51] J. M. Luttinger, Phys. Rev. **119**, 1153 (1960).